

# Computational Analysis of Aluminum Corrosion Inhibition Potentials Using Selected Thiosemicarbazide Derivatives

## ABSTRACT

Aluminum, a metal with a rich cultural history, remains vital in numerous industrial applications. However, its susceptibility to corrosion in harsh environments poses significant challenges. Traditional corrosion inhibitors have been developed to counteract this issue, but they often come with drawbacks such as high costs and harmful environmental and health impacts. This study employed density functional theory (DFT) to evaluate the potential of two compounds—2-(4-methylbenzylidene)hydrazinecarbothioamide (MBHC) and N-phenylhydrazinecarbothioamide (PHC)—as corrosion inhibitors for aluminum surfaces. Electrostatic potential (ESP) analysis revealed that the sulphur and nitrogen atoms in these compounds exhibit nucleophilic behaviour, making them effective for corrosion inhibition. The research highlighted MBHC's superior performance over PHC in corrosion prevention. Molecular orbital theory and Monte Carlo simulations demonstrated that MBHC formed stronger and more stable complexes with the aluminum surface, as reflected in its higher adsorption energy of  $-461.73$  eV compared to PHC's  $-163.43$  eV. These findings pave the way for developing environmentally friendly inhibitors to protect aluminum surfaces, combining efficiency with sustainability.

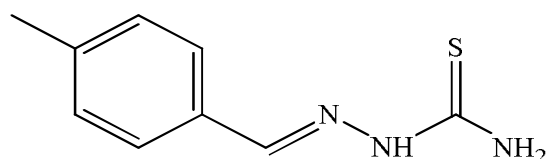
*Keywords: adsorption energy; DFT; Potentials; Aluminum; inhibitor; Simulation*

## 1. INTRODUCTION

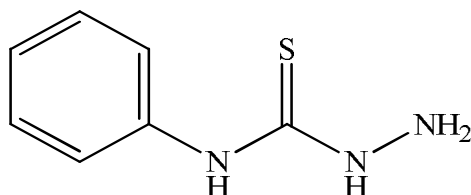
In the crust of the globe, aluminum is the third most frequent metal overall and the fourth most prevalent in the crust specifically. After iron, aluminum is typically regarded as the second most significant metal. It has unique mechanical characteristics because of its low density ( $2.7 \text{ g cm}^{-3}$ ), which is just about one-third that of mild steel. As a result, aluminum and its alloys offer a high strength-to-weight ratio. In addition, a wide range of metal machining processes can be readily applied to them, and they exhibit good electrical and thermal conductivity. Furthermore, aluminum and its alloys have been fully recycled and reused, meaning that the items made from recycled metal are similar to those that were made before recycling in terms of quality and attributes (Olufumilayo & Olakunle, 2021). Because of its excellent strength-to-weight ratio and affordable price, aluminum and its alloys are widely used in aerospace, automotive, electrical parts, building, packaging, and chemical industries (Rouniya & Shandilya, 2019; Becker, 2019; Emadi et al., 2019). In non-aggressive conditions, an  $\text{Al}_2\text{O}_3$  coating naturally forms on the alloy surface to preserve aluminum (Arrousse et al., 2022). Because of its numerous flaws and pores, the oxide layer is rapidly dissolved by corrosive  $\text{OH}^-$  or  $\text{Cl}^-$  ions. However, because key alloy components like copper and magnesium are present, aluminum and its alloys are highly susceptible to localized corrosion in harsh conditions. This alloy's microstructure is rather complicated, and several phases with different compositions have been found (Liu et al., 2017). Since an

oxide layer forms on aluminum and prevents the metal from oxidizing further, aluminum has a high level of corrosion resistance in both aqueous solutions and the environment. However, in some conditions, such as acidic media, aluminum becomes extremely prone to corrosion. There are already several efficient protection techniques available, including surface coatings, organic inhibitor addition, anodic oxidation protection, and plasma electrolytic oxidation protection (Gummanar et al., 2023; Markus, 2019; Yang et al., 2017). Inhibitors, which prevent corrosion on metal surfaces by forming a protective coating on them, are the most widely used and least expensive of them across a variety of industries. Products with an organic base are frequently used to prevent corrosion. Organic compounds with heteroatoms (N, S, and O) in a conjugated system exhibit excellent efficacy in preventing metal corrosion (Verma et al., 2016; Iroha & Akaranta, 2020; Nkem et al., 2021). The effectiveness of corrosion inhibition has been precisely established by experimental research, however, the precise mechanism by which inhibitors contribute most to corrosion inhibition has not been thoroughly addressed. Costs and time for research are significant. These issues are bridged by the theoretical study, which is now backed by sufficient hardware and software. The electron density of the molecule determines the corrosion inhibition efficiency, and theoretical research can determine this density with high accuracy. When evaluating corrosion inhibition in a molecule, theoretical research is just as important as actual research. Questions concerning experimental results based on the interactions of organic inhibitors with metal surfaces can be addressed using quantum chemical computations (Ebenso et al., 2021). Verma et al. (Verma et al., 2021) underlined in their thorough review the application of quantum chemistry techniques to corrosion inhibitor investigations of several organic compounds. Uzah, (2024) theoretically explored the interactions between selected thiosemicarbazide derivatives on Al (111) and Cu (111) surfaces by using the B3LYP/6-311G (d, p) method. The Electrostatic potential (ESP) surface analysis used to identify the reactive areas., was considered, and Fukui indices were determined for N+1 and N-1 electron species, at the geometry of the selected thiosemicarbazide derivatives reference N-electron. Their results showed that the  $\Delta E$ ,  $E_{LUMO}$ ,  $\chi$ ,  $\eta$ ,  $E_{HOMO}$ ,  $\sigma$ , and  $\Delta N$  localization and the condensed Fukui functions (f- and f+) analysis in the reactive region were instrumental in characterizing organic adsorbates. Ibrahim et al. (2023) investigated the potentiality of the 6-mercaptopurine (MP) and 6-thioguanine (TG) expired drugs toward the corrosion inhibition of the aluminum (Al) (111) surface, using the B3LYP/6-311G basis set.  $\Delta E$ ,  $E_{HOMO}$ ,  $E_{LUMO}$ ,  $\mu$ , and  $\eta$  parameters were all calculated for each of the expired drugs, both in the liquid and gas phases, of which results show no significant difference in the structures of the expired drugs. Khabazi and Chermahini, (2023) presented Two different isomeric forms of tetrazole molecules and their derivatives, including 1H and 2H tautomers, as corrosion inhibitors were studied in two configurations, parallel and perpendicular to the Cu (1 1 1) surface, using the 6-31GDFT method. The Mulliken partial charges,  $E_{HOMO}$ ,  $E_{LUMO}$ ,  $\Delta E$ , total hardness ( $\eta$ ), electronegativity ( $\chi$ ), and electron fraction transitions from the anti-corrosion molecule to the copper atom ( $\Delta N$ ), were, calculated, and the IE was associated with  $\Delta E$  and the frontier orbital electron density. It was observed that tetrazole molecules were physically adsorbed onto the copper surface. The performance of each inhibitor concerning its structure and orientation, as well as the mechanism by which an inhibitor clings to metal surfaces, may be fully explained by the use of the methods of density functional theory and Monte Carlo simulation (Sulaiman et al., 2019). Hadisaputra et al., (2022) investigated the real environment conditions of corrosion inhibition in the solution phase can be replicated by the Monte Carlo simulation. The corrosion inhibition efficiency of phthalimide derivatives was PP-OCH3 > PP-CH3 > PP-H > PP-Cl > PP-NO2. The theoretical study was consistent with previously reported experimental results. The surface interactions between the inhibitor molecules and the metal surface were investigated by Oukhrib et al., (2021) using molecular dynamics simulations and Monte Carlo (MC) simulations. As a result, they found that the inhibitor pyrazolynucleosides have

89 strong interactions with Cu (111) surface, and therefore have excellent predictive inhibition  
 90 power against copper corrosion. Derivatives of thiosemicarbazide are widely used in medical  
 91 chemistry to create medications that combat germs, fungi, viruses, depression, etc. Its  
 92 primary biological functions are DNA doping transporter, anticancer, and DNA retaining  
 93 capacity. No computational study has been published on the corrosion prevention of MBHC  
 94 and PHC derivatives of Thiosemicarbazide on Aluminium Surfaces. However, some of these  
 95 derivatives are said to be effective deterioration inhibitors for Aluminium in acidic media. The  
 96 corrosion inhibition of MBHC and PHC (Fig.1): on Al (111) surfaces are studied in this work,  
 97 along with the impacts of quantum parameters and the molecule's adsorption process.



98 *(E)*-2-(4-methylbenzylidene)hydrazinecarbothioamide (MBHC)



99 *N*-phenylhydrazinecarbothioamide (PHC)

100 **Fig.1. The chemical structures of MBHC and PHC**

101  
 102 **2. COMPUTATIONAL DETAILS**

103  
 104 **2.1 DFT Study**

105  
 106 Studies on corrosion inhibition commonly employ the density functional theory (DFT). When  
 107 it comes to organic compounds' ability to suppress corrosion, the DFT approach provides an  
 108 accurate description. Predicting the chemical properties of chemical species, such as the  
 109 maximum occupied molecular orbital–lowest unoccupied molecular orbital (HOMO–LUMO),  
 110 electron affinity (A), ionization potential (I), energy gap ( $\Delta E$ ), hardness ( $\eta$ ), fraction of  
 111 electrons transferred ( $\Delta N$ ), softness ( $\sigma$ ), and electronegativity ( $\chi$ ), is the main goal of  
 112 research on inhibitors. The following paper used theoretical calculations to anticipate the  
 113 effectiveness of the Thiosemicarbazide derivatives *E*-2-(4-  
 114 methylbenzylidene)hydrazinecarbothioamide (MBHC) and *N*-  
 115 phenylhydrazinecarbothioamide (PHC) (Fig.1). Employing the Gaussian 09W programming  
 116 suite, the B3LYP technique coupled to 6-311G+ (d,p) basis sets were utilized to optimize all  
 117 compounds geometrically. This approach is widely used in the research of organic corrosion  
 118 inhibitors. Then, several relevant global and local variables of the molecule's electronic  
 119 configuration were computed. The I, A,  $\Delta E$ ,  $\Delta N$ ,  $\eta$ ,  $\sigma$ ,  $\chi$ ,  $E_{LUMO}$ , and  $E_{HOMO}$  as well as maps of  
 120 electrostatic potential were also computed (Verma et al., 2021; Khabazi&Chermahini,2023).

121 
$$A = E_{LUMO} \quad (1)$$

122 
$$I = E_{HOMO} \quad (2)$$

123 
$$\Delta E = E_{LUMO} - E_{HOMO} \quad (3)$$

124 
$$\eta = \left(\frac{\delta^2 E}{\delta N^2}\right)_v = \left(\frac{\delta \mu}{\delta N}\right)_v = \frac{E_{LUMO} - E_{HOMO}}{2} \quad (4)$$

125 
$$\sigma = 2 \left( \frac{\delta N}{\delta \mu} \right)_{v(r)} = \frac{1}{\eta} = \frac{2}{\Delta E E_{LUMO} - E_{HOMO}} \quad (5)$$

126 
$$\chi = \frac{-(E_{HOMO} + E_{LUMO})}{2} \quad (6)$$

127 
$$\Delta N = \frac{(\chi_{Al} - \chi_{inh})}{2 \times (\eta_{Al} - \eta_{inh})} \quad (7)$$

128 Where,  $\chi_{Al} = 4.26$  eV and  $\chi_{inh}$  = absolute electronegativities of the aluminum and inhibitor  
 129 respectively.  $\eta_{Al} = 0$  eV and  $\eta_{inh}$  = absolute hardness of the aluminum and inhibitor  
 130 respectively.

131 **2.2 Monte Carlo simulation.**

132

133 The interactions between the chemical compounds and metal surface were theoretically  
 134 studied by the Monte Carlo simulation The simulation was conducted in Material Studio 2020  
 135 (Biovia, USA) using COMPASS force-field (condensed phase), on the Al (111) surface (three  
 136 dimensions to the slab model) under periodic boundary conditions. The energies and  
 137 chemical adsorption mechanisms components were calculated using the Ewald and atom-  
 138 based summations, or responsibly to the Adsorption Locator module, built-in Materials  
 139 Studio 2020 which used Monte Carlo simulations to pinpoint the most stable arrangement of  
 140 the adsorbates on the Al (111) surface is the most stable of the many aluminum surfaces  
 141 (Bourzi et al., 2020; Uzah, & Mbonu, 2023),

142

143 **3. RESULTS AND DISCUSSION**

144

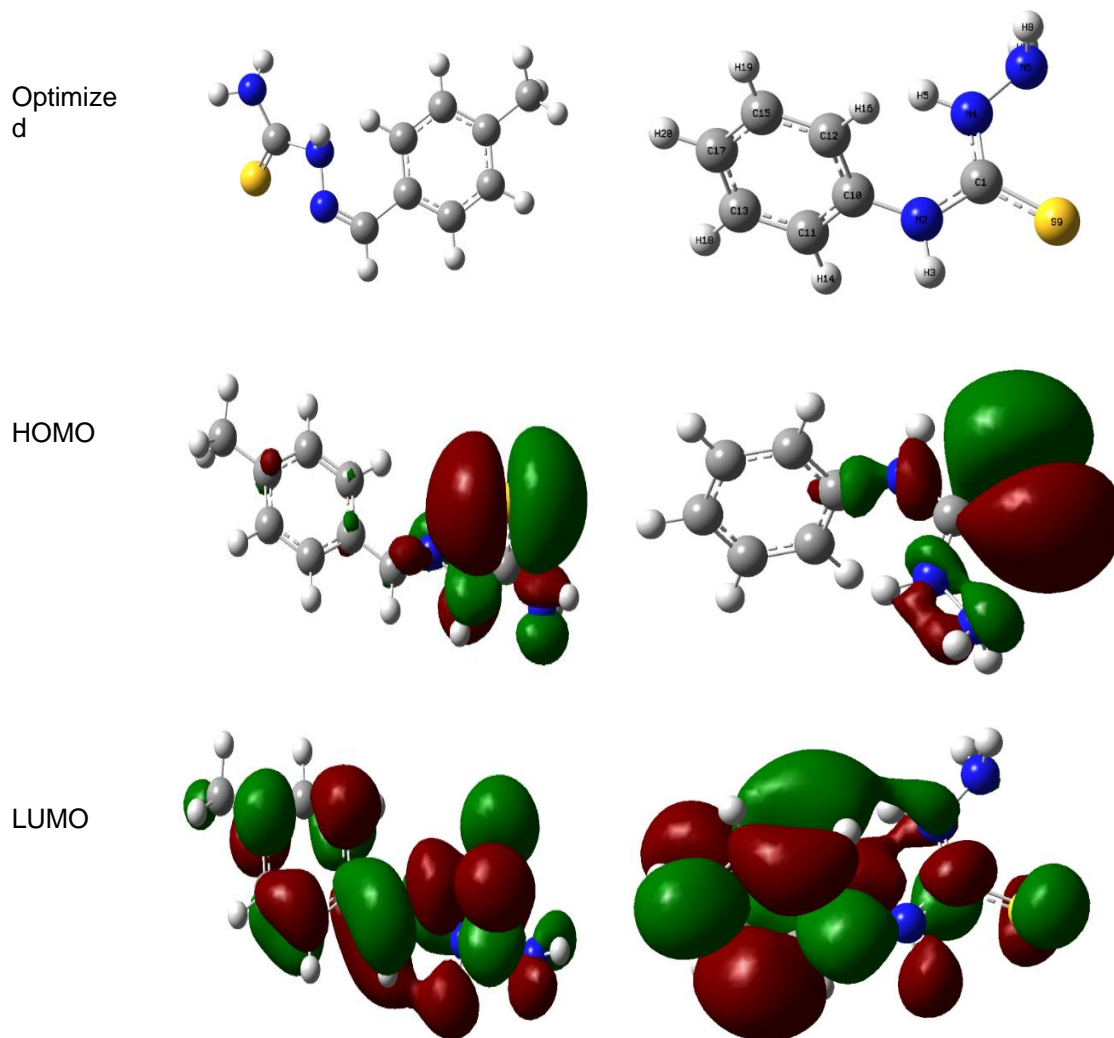
145 **3.1. DFT Results**

146

147 Table 1 is a list of the calculated quantum chemical parameters. Given structures that are  
 148 optimized HOMO and LUMO density distribution of PHC and MBHC, Fig.2 shows that PHC  
 149 has fewer adsorption centers than MBHC, indicating that MBHC has a higher capacity for  
 150 high-protective adsorption. As a result, the high  $E_{HOMO}$  energy increases the inhibition  
 151 performance by reflecting a greater connection between the molecule and the metal surface  
 152 through the donor-acceptor process. (Guo et al., 2017; Hadisaputra et al., 2022). MBHC can  
 153 readily interchange electrons with the iron surface, as evidenced by its higher  $E_{HOMO}$  value of  
 154  $-0.218$  eV compared to PHC's  $-0.210$  eV. On the other hand, the fact that MBHC has a  
 155 lower  $E_{LUMO}$  value indicates that it is an excellent inhibitor of electron acceptance and  
 156 supports its superior performance ( $-0.018$  eV) over PHC ( $-0.042$  eV)  
 157 (Khabazi&Chermahini,2023; Uzah& Mbonu, 2024). Better adsorption on aluminum surfaces  
 158 is indicated by the narrower energy gap ( $\Delta E$ ) of MBHC ( $0.1493$  eV) (Fouda et al., 2023).  
 159 Further quantum chemical characteristics were derived, including ionization potential ( $I =$   
 160  $-E_{HOMO}$ ), electron affinity ( $A = -E_{LUMO}$ ), global softness ( $\sigma$ ), global hardness ( $\eta$ ),  
 161 electronegativity ( $\chi$ ), and number of electron transfer ( $\Delta N$ ). The literature claims that a  
 162 molecule with a high ( $\eta$ ) value is less reactive, whereas a high ( $\chi$ ) value indicates that the  
 163 molecule may find it difficult to transfer its electrons to an acceptor (Kaya & Kaya, 2015;  
 164 Uzah et al., 2023). The findings in Table 1 demonstrate that MBHC has lower ( $\eta$ ) and ( $\chi$ )  
 165 values than PHC, indicating that it is more reactive and can transfer electrons through donor-  
 166 acceptor interactions with metal molecules. (Uzah,2024). Within a group of inhibitors, the  
 167 electron donation tendency is described by the charge transfer rate  $\Delta N$ . According to  
 168 Lukovits ((Jabri et al., 2022; Uzah et al., 2023), the efficiency of the inhibition increases as  
 169 the electron donor capacity at the steel/electrolyte increases if  $\Delta N < 3.6$ . Table 1 displayed  
 170  $\Delta N$  values are all 3.6 lower than the original values. Therefore, the quantum chemical  
 171 characteristics of MBHC performed better at its level of inhibition than the PHC inhibitor.

172

Inhibitor	MBHC	PHC
-----------	------	-----



173 Fig.2. The frontier molecular orbital density distribution for MBHC and PHC  
174 investigated compounds (Optimized, HOMO, and LUMO).  
175

176

177

178

179 Table 1. The quantum chemical variables for MBHC and PHC inhibitors using  
the B3LYP/6-31G+ (d, p) basis set.

C	$E_{LUMO}$	$E_{HOMO}$	$\Delta E$	H	$\Sigma$	X	$\Delta N_{AI}$
MBHC	-0.0180	-0.2178	0.1493	0.0747	13.40	0.143	-20.66
PHC	-0.0422	-0.2095	0.1673	0.0837	11.95	0.0948	-18.54

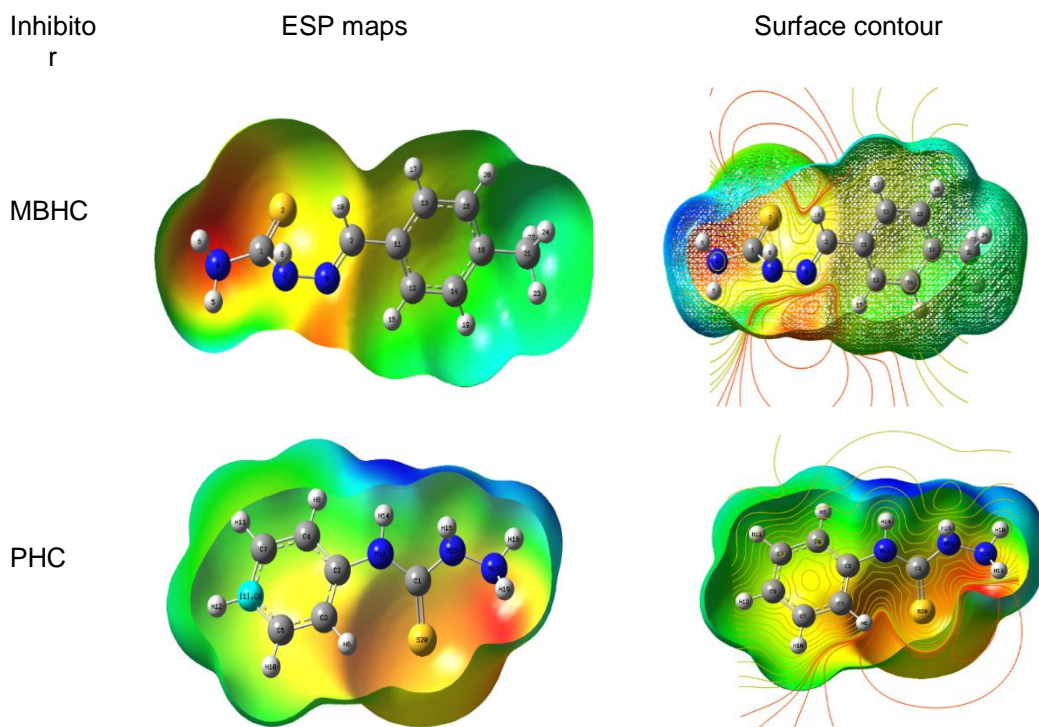
180

### 181 3.2 Electrostatic Potential (ESP) Map

182

183 ESP map displays the three-dimensional charge distribution of the molecule (Fig.3). This  
184 map aids in the visualization of the molecule's variable charge areas, which helps forecast  
185 electrophilic and nucleophilic molecule-attack scenarios (Thakur & Kumar, 2023). The

186 highest positive region vulnerable to nucleophile assault is shown as blue in the ESP plot.  
187 On the other hand, the negative region that is vulnerable to electrophilic attack is shown in  
188 red. The MBHC and PHC sulfur and nitrogen atoms are found to have the highest electron  
189 density. Consequently, it is expected that these atoms will actively participate in the  
190 adsorption process on the Aluminum surface.  
191  
192  
193



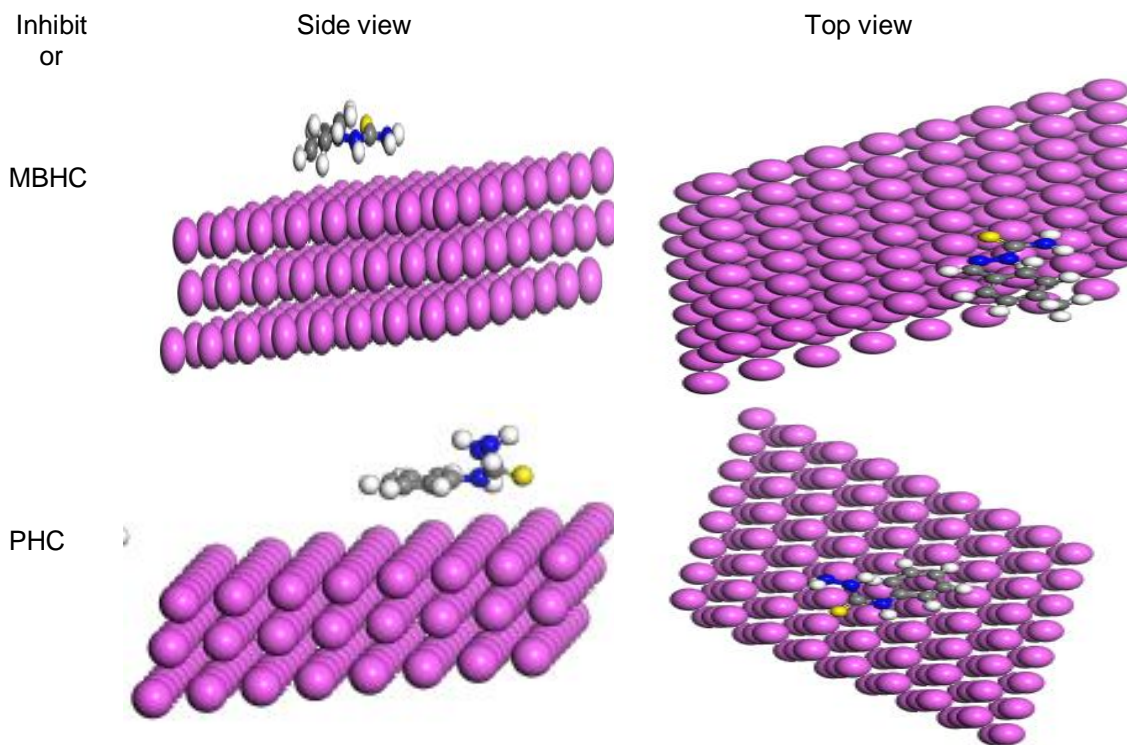
194 **Fig.3. ESP maps and surface contours illustration of the MBHC and PHC**  
195 **investigated**

### 196 197 **3.3 Monte Carlo simulation.** 198

199 To reduce the amount of contact area between the metal surface and corrosion-causing  
200 materials (such as water, acidic, or alkaline media), molecules need to align their structures  
201 as closely as possible in parallel to the metal surface. Adsorption is the term for this process.  
202 Therefore, Monte Carlo simulation was applied to determine and identify the inhibitors under  
203 evaluation and their ability to adsorb onto the surface of Al (111). Fig.4 shows the optimal  
204 MBHC and PHC adsorption mode on the aluminum surface under study.

205 Table 2 displays the molecule under investigation's adsorption characteristics, which include  
206 total energy, rigid adsorption energy, adsorption energy, and deformation energy. We have  
207 previously defined these parameters (Bourzi et al., 2020; Uzah, 2025). in our previous work.  
208 The total rigid adsorption energy before and after an adsorbate's surface relaxation is known  
209 as the "adsorption energy," and it is the most significant energy characteristic in adsorption.  
210 Table 2 indicates that the inhibitor attaches to the surface of Al (111) spontaneously based  
211 on the negative value of the adsorption energies (Uzah, & Mbonu, 2023). The differential

212 adsorption energy ( $dE_{ad}/dN_i$ ), which is the energy needed or released to remove a portion of  
 213 the adsorbate (i.e., desorption energy), is defined by assuming that the surface energy of Al  
 214 is zero. The inhibitor's adsorption energy of  $-461.73 \text{ kcal mol}^{-1}$  for MBHC and  $163.43 \text{ kcal mol}^{-1}$   
 215  $\text{mol}^{-1}$  for PHC and its desorption energy of  $--461.73 \text{ kcal mol}^{-1}$  (MBHC) and  $-80.754 \text{ kcal}$   
 216  $\text{mol}^{-1}$  (PHC) indicate that the adsorption process is substantially preferred. The inhibitor  
 217 preferentially adsorbs on the Al (111) surface with little to no competition because it adsorbs  
 218 with significantly less energy, even in the presence of water ( $--4.28 \text{ kcal mol}^{-1}$ ) (Benzidia et  
 219 al., 2022; Uzah, 2025).  
 220  
 221



222  
 223 **Fig.4. The most appropriate conformation for adsorption of the MBHC and PHC**  
 224 **molecules on Al (111)**  
 225  
 226  
 227  
 228

229 **Table 2. Results and descriptors measured by the Monte Carlo simulation for**  
 230 **adsorption of MBHC and PHC molecules on Al (111)**  
 231

Compound	$dE_{ad}/dN_i$	Adsorption energy	Rigid adsorption energy	Deformation energy	Total energy
MBHC	-461.73	-461.73	-30.707	-431.02	-3.272
PHC	-80.75	-163.43	-55.83	-107.61	-5.75
Water	-4.281	-8.297	-7.346	-0.950	-7.346

232

233 **4. CONCLUSION**

234

235 The corrosion inhibition potential of E)-2-(4-methylbenzylidene)hydrazinecarbothioamide  
236 (MBHC) and N-phenylhydrazinecarbothioamide (PHC) was analyzed and measured using  
237 density functional theory calculations employing the B3LYP/6-31G+ (d,p) basis set. This was  
238 done to determine whether these compounds had a potentially strong ability to inhibit  
239 corrosion in aluminum and its alloys. In contrast to PHC, MBHC has a lower electronegativity  
240 and  $\Delta E$ , (0.1612 eV) values, which may be attributed to the presence of an aromatic ring and  
241 heteroatom in its structure, which demonstrated a stronger and mutual connection between  
242 the inhibitor and the metallic surface according to the results of the Density Functional  
243 Theory analysis: Furthermore, the results showed that MBHC had the largest  $\Delta N$  value  
244 (0.258232 eV), indicating improved chemical stability and reactivity. In light of this, MBHC is  
245 more likely than PHC to react as an electron donor, which effectively inhibits the  
246 corrosion of alloys including aluminum. MBHC was predicted by Monte Carlo simulations to  
247 function as a more potent anti-corrosion agent than PHC, particularly in acidic environments.  
248

249 **DISCLAIMER (ARTIFICIAL INTELLIGENCE)**

250 Authors hereby declare that NO generative AI technologies such as Large Language Models  
251 (ChatGPT, COPILOT, etc.) and text-to-image generators have been used during the writing  
252 or editing of this manuscript.

253 **ACKNOWLEDGEMENTS**

254

255 The authors would like to acknowledge the Federal University of Petroleum Resources,  
256 Effurun for creating an enabling environment for this research work.

257

258

259

**COMPETING INTERESTS**

260 **Competing interests** The authors declare no conflict of interest.

261

262 **AUTHORS' CONTRIBUTIONS**

263

264 The manuscript was written with contributions from all authors. All authors read and approved  
265 the final manuscript

266

267

268

**REFERENCES**

269

270

271

272

273

274

275

276

277

278

1. Arrousse, N., Fernine, Y., Al-Zaqri, N., Boshala, A., Ech-chihbi, E., Salim, R., El Hajjaji, F., Alami, A., EbnTouhamie, M., Taleb, M. (2022). Thiophene derivatives as corrosion inhibitors for 2024-T3 aluminum alloy in hydrochloric acid medium. *RSC Advances*, 12, 10321. DOI: 10.1039/d2ra00185c
2. Becker, M. (2019). Chromate-free chemical conversion coatings for aluminum alloys, *Corrosion Review*, 37, 321–342. <https://doi.org/10.1515/correv-2019-0032>
3. Benzidia, B., Barbouchi, M., Hsissou, R., Zouarhi, M., Erramli, H., Hajjaji, N. (2022). A combined experimental and theoretical study of green corrosion inhibition of bronze B66 in 3% NaCl solution by Aloe saponaria (syn. Aloe maculata) tannin extract. *Current Research in Green and Sustainable Chemistry*, 5, 100299. <https://doi.org/10.1016/j.crgsc.2022.100299>



- 279  
280  
281  
282  
283  
284  
285  
286  
287  
288  
289  
290  
291  
292  
293
4. Bourzi, H., Oukhrib, R., El Ibrahim, B., Oualid, H. A., Abdellaoui, Y., Balkard, B., El Issami, S., Hilali, M., Bazzi, L., Len, C. (2020). Furfural analogs as sustainable corrosion inhibitors—predictive efficiency using DFT and Monte Carlo simulations on the Cu (111), Fe (110), Al (111) and Sn (111) surfaces in acid media. *Sustainability*, 12, 3304; doi:10.3390/su12083304
5. Ebenso, E. E., Verma, C., Olasunkanmi, L. O., Akpan, E. D., Verma, D. K., Lgaz, H., Quraishi, M. A. (2021). Molecular modeling of compounds used for corrosion inhibition studies: a review. *Physical Chemistry Chemical Physics*, 23, 19987–20027. <https://doi.org/10.1039/D1CP00244>
6. Emadi, M., Beheshti, H., Heidari-Rarani, M., Aboutalebi, F. H. (2019). Experimental study of collapse mode and crashworthiness response of tempered and annealed aluminum tubes under axial compression, *Journal of Mechanical Science and Technology*, 33, 2067–2074. <http://dx.doi.org/10.1007/s12206-019-0410-2>
7. Fouda, A. S., Etaiw, S. H. E., Ibrahim, A. M., El-Hossianya, A. A. (2023). Insights into using two novel supramolecular compounds as corrosion inhibitors for stainless steel in a chloride environment: experimental and theoretical investigation. *RSC Advance*, 13, 35305–35320. <https://doi.org/10.1039/d3ra07397a>
- 294  
295  
296  
297  
298  
299  
300  
301  
302  
303  
304
8. Gummanar, N., Mokshanatha, P. B., Dyapur, P., Yallappa, G. N. (2023). Organic corrosion inhibitors for aluminum-based alloys –A Review. *Letters in Applied NanoBioScience*, 12, 4, 170. <https://doi.org/10.33263/LIANBS124.170>
9. Guo, L., Obot, I. B., Zheng, X., Shen, X., Qiang, Y., Kaya, S., Kaya, C. (2017). Theoretical insight into an empirical rule about organic corrosion inhibitors containing nitrogen, oxygen, and sulfur atoms, *Applied Surface Science*, 406, 301–306. <http://dx.doi.org/10.1016/j.apsusc.2017.02.134>
10. Hadisaputra, S., Purwoko, A. A., Hakim, A., Prasetyo, N., Hamdiani, S. (2022). Corrosion inhibition properties of phenyl phthalimide derivatives against carbon steel in the acidic medium: DFT, MP2, and Monte Carlo simulation studies. *ACS Omega*, 7, 33054–33066. <https://doi.org/10.1021/acsomega.2c03091>
- 305  
306  
307  
308  
309
11. Ibrahim, M.A.A., Moussa, N.A.M., Mahmoud, A.H.M., Sayed, S.R.M., Sidhom, P.A., Abd El-Rahman, M.K., Shoeib T., Mohamed, L.A., (2023). Density functional theory study of the corrosion inhibition performance of 6-mercaptopurine and 6-thioguanine expired drugs toward the aluminium (111) surface. *RSC Advances*, 13, 29023–29034. <https://doi.org/10.1039/d3ra04954j>
- 310  
311  
312  
313
12. Iroha, N. B., Akaranta, O. (2020). Experimental and surface morphological study of corrosion inhibition of N80 carbon steel in HCl stimulated acidizing solution using gum exudate from Terminalia Mentaly. *SN Applied Sciences*, 2, 1514, <https://doi.org/10.1007/s42452-020-03296-8>.
- 314  
315  
316  
317  
318
13. Jabri, Z., El Ibrahim, B., Jarmoni, K., Sabir, S., Misbahi, K., Rodi, Y. K., Mashrai, A., Hökelek, T., Mague, J. T., Sebbar, N. K., Essassi, E. (2022). New imidazo[4,5-b] pyridine derivatives: synthesis, crystal structures, Hirschfeld surface analysis, DFT computations, and Monte Carlo simulations. *Journal of Chemical Technology and Metallurgy*, 57(3), 451- 463. <https://doi.org/10.2174/0929867330666230426111650>
- 319  
320  
321
14. Kaya, S., Kaya, C. (2015). A new method for calculation of molecular hardness: A theoretical study, *Computational and theoretical chemistry*, 1060, 66. <https://doi.org/10.1016/j.comptc.2015.03.004>
- 322  
323  
324
15. Khabazi, M. E., Chermahini, A. N. (2023). DFT study on corrosion inhibition by tetrazole derivatives: investigation of the substitution effect. *ACS Omega*, 8, 9978–9994. <https://doi.org/10.1021/acsomega.2c07185>
- 325  
326  
327
16. Liu, Y., Li, X. L., Jin, J. F., Liu, J. A., Yan, Y. Y., Han, Z. W., Ren, L. Q. (2017). Anti-icing property of bioinspired microstructure superhydrophobic surfaces and heat transfer model, *Applied Surface Science*, 400, 498–505. <https://doi.org/10.1016/j.apsusc.2016.12.219>
- 328  
329
17. Markus, B. (2019). Chromate-free chemical conversion coatings for aluminum alloys. *Corrosion Review*, 37, 32-39, <https://doi.org/10.1515/corrrev-2019-0032>.

- 330 18. Nkem, B., Iroha, N. B., Maduelosi, N. J. (2021). Corrosion inhibitive action and adsorption  
331 behavior of *justicia secunda* leaves extract as an eco-friendly inhibitor for aluminum in acidic  
332 media. *Biointerface Research in Applied Science*. 11 (5), 13019 – 13030.  
333 <https://doi.org/10.33263/BRIAC115.1301913030>
- 334 19. Olufumilayo, O. J., Olakunle, O. J. (2021). Corrosion inhibition of Aluminum alloy by chemical  
335 inhibitors: An overview. *IOP Conference Series: Material Science and Engineering*, 1107,  
336 012170. <https://doi.org/10.1088/1757-899X/1/012170>.
- 337 20. Oukhrib, R., Abdellaoui, Y., Berisha, A., Oualid, H.A., Halili, J., Jusufi, K., El Had, M.A., Bourzi,  
338 H., El Issami, S., Asmary, F.A., Parmar, V.S., Len, C. (2021) DFT, Monte Carlo and molecular  
339 dynamics simulations for the prediction of corrosion inhibition efficiency of novel  
340 pyrazolylnucleosides on Cu(111) surface in acidic media. *Scientific Reports*, 11, 3771.  
341 <https://doi.org/10.1038/s41598-021-82927-5>.
- 342 21. Rouniya, A. K., Shandilya, P. (2019). Fabrication and experimental investigation of magnetic  
343 field assisted powder mixed electrical discharge machining on machining of aluminum 6061  
344 alloys, *Proceeding of the Institution of Mechanical Engineer Part B Journal of Engineering*  
345 *Manufacturer*, 233, 2283–2291.
- 346 22. Sulaiman, K. O., Onawole, A. T., Faye, O., Shuaib, D. T. (2019). Understanding the corrosion  
347 inhibition of mild steel by selected green compounds using chemical quantum-based  
348 assessments and molecular dynamics simulations. *Journal of Molecular Liquids*, 279, 342–350.  
349 <http://dx.doi.org/10.1016/j.molliq.2019.01.136>
- 350 23. Thakur, A., Kumar, A. (2023). Computational insights into the corrosion inhibition potential of  
351 some pyridine derivatives: A DFT approach. *European Journal of Chemistry*, 14(2), 246-253.  
352 <https://dx.doi.org/10.5155/eurjchem.14.2.246-253.2408>
- 353 24. Uzah, T. T., Mbonu, I. J. (2023). Insight into synergistic corrosion inhibition of thiourea and ZnCl<sub>2</sub>  
354 on mild steel: Experimental and theoretical Approaches. *Journal of Chemistry Letters*, 4, 211-  
355 221. <https://doi:10.22034/jchemlett.2024.413932.1135>
- 356 25. Uzah, T. T., Mbonu, J. I. (2024). Enhancing the inhibition action of acetamide with iodide ions for  
357 mild steel corrosion in 0.5 M H<sub>2</sub>SO<sub>4</sub> environment. *Letters in Applied NanoBioScience*, 13, 1-16,  
358 <https://doi.org/10.33263/LIANBS131.049>.
- 359 26. Uzah, T. T., Mbonu, J. I., Gber, T. E., Louis, H. (2023). Synergistic effect of KI and urea on the  
360 corrosion protection of mild steel in 0.5 M H<sub>2</sub>SO<sub>4</sub>: Experimental and computational insights.  
361 *Results in Chemistry*, 5, 1-9. <https://doi.org/10.1016/j.rechem.2023.100981>
- 362 27. Uzah, T.T. (2025) Theoretical evaluation of urea derivatives on Fe (110) and Sn (111) surfaces  
363 in acidic medium: DFT and Monte Carlo simulation approaches. *Materials International*. 7(1), 1-  
364 12 <https://doi.org/10.33263/Materials71.002>
- 365 28. Uzah, T. T. (2024). DFT and Monte Carlo simulation for the prediction of corrosion inhibitive  
366 efficacy of selected thiosemicarbazide derivatives on Al (111) and Cu (111) Surfaces in Acidic  
367 Media. *Journal of Medical and Nanomaterial Chemistry*, 6, 81-94,  
368 <https://doi.org/10.48309/JMNC.2024.1.7>
- 369 29. Verma, C., Olasunkanmi, L. O., Ebenso, E. E., Quraishi, M. A., Obot, I. B. (2016). Adsorption  
370 behavior of glucosamine-based, pyrimidine-fused heterocycles as green corrosion inhibitors for  
371 mild steel: Experimental and Theoretical Studies. *The Journal of Physical Chemistry C*, 120,  
372 11598-11611, <https://doi.org/10.1021/acs.jpcc.6b04429>.
- 373 30. Verma, D. K., Aslam, R., Aslam, J., Quraishi, M. A., Ebenso, E. E., Verma, C. (2021).  
374 Computational modeling: theoretical predictive tools for designing of potential organic corrosion  
375 inhibitors. *Journal of Molecular Structures*, 1236, 130294.  
376 <https://doi.org/10.1016/j.molstruc.2021.130294>
- 377 31. Yang, W., Xu, D., Chen, J., Liu, J., Jiang, B. (2017). Characterization of self-sealing MAO  
378 ceramic coatings with green or black color on an Al alloy. *RSC Advances*, 7, 1597-1605,  
379 <https://doi.org/10.1039/C6RA25415B>.

